ACS OMEGA

Open Access

http://pubs.acs.org/journal/acsodf

Article

Photocatalytic and Antimicrobial Properties of ZnO and Mg-Doped ZnO Nanoparticles Synthesized Using *Lupinus albus* Leaf Extract

Abdu Muhammed, Tsegaye Girma Asere,* and Tamiru Fayisa Diriba

Cite This: *ACS Omega* 2024, 9, 2480−2490

Read Online

ACCESS | Metrics & More | Article Recommendations

ABSTRACT: Dye effluents discharged from various industries contribute to environmental contamination, making their treatment highly necessary. Infectious diseases also pose a threat to public health worldwide. Nanomaterials have promising features and are potential candidates for overcoming the problems of drug resistance in microbes and environmental pollution. Therefore, this study aimed to synthesize zinc oxide (ZnO) and magnesium-doped zinc oxide (Mg-doped ZnO) nanoparticles (NPs) using the plant extract of *Lupinus albus* for applications in photocatalysis and antimicrobial activity. A sample of *Lupinus albus* leaves was collected from Motta, in the eastern Gojjam zone of Ethiopia. The leaves were air-dried and then ground into a powder. The powdered plant material was extracted using distilled water. The ZnO and Mg-doped ZnO NPs were synthesized using 0.1 M $Zn(NO_3)_2{\cdot}6H_2O$, 7.5% 0.1 M $Mg(NO_3)2.6H_2O$, and 10 mL of the leaf extract. The nanoparticles (NPs) were characterized using UV−vis, FT-IR, XRD, and SEM. The average crystallite sizes of ZnO and Mg-doped ZnO NPs were determined using the Debye−Scherrer formula and were found to be 28.1 and 34.4 nm, respectively. The antimicrobial activity of the synthesized NPs was evaluated against four bacterial strains (*Escherichia coli*, *Bacillus cereus*, *Salmonella typhi*, and *Staphylococcus aureus*) and one fungal strain (*Candida albicans*) by using the agar disk diffusion method. The Mg-doped ZnO NPs exhibited significant antimicrobial activity, with a maximum zone of inhibition measuring 24 and 22 mm against *Escherichia coli* and *Salmonella typhi*, respectively. The photocatalytic activity of ZnO and Mg-doped ZnO NPs was investigated by studying the degradation of methylene blue (MB) dye under sunlight irradiation for 120 min. The results showed that Mg-doped ZnO NPs exhibited higher photocatalytic activity (99.6%) than ZnO NPs (94.1%). In conclusion, the synthesized NPs could serve as viable alternatives for antimicrobial drugs and photocatalysts to mitigate the pollution of the environment caused by organic dyes.

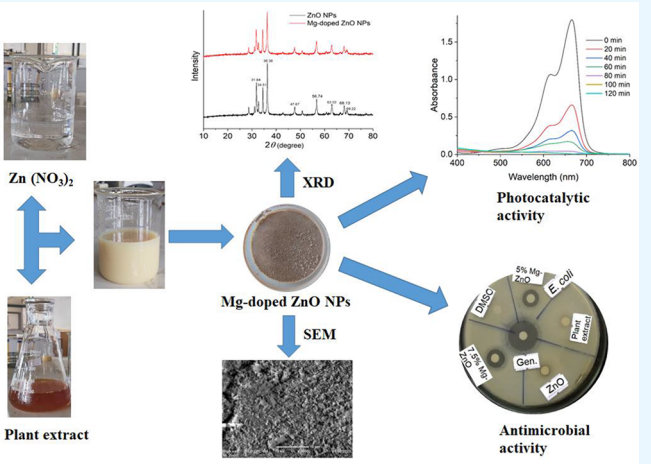

1. INTRODUCTION

The prevailing rates of disease prevalence and mortality worldwide are primarily associated with environmental pollutants and drug-resistant microorganisms. These factors have been identified as significant contributors to the occurrence of both noncommunicable and infectious diseases. The discharge of dyes from the textile and paper industries is widely recognized for its high toxicity and carcinogenic properties, thus presenting a substantial environmental hazard. Despite the extensive research and development efforts focused on enhancing dye treatment methods, the cost-effective removal of dyes from wastewater remains a formidable obstacle.[1,2] Therefore, the development of treatment technologies that are both economically viable and ecologically sustainable is of the utmost significance. Recently, there has been notable emphasis on nanoparticles (NPs) in the field of photocatalytic application. A nanoparticle is a particle with a small size, typically ranging from 1 to 100 nm. Scientists have synthesized NPs in different ways such as physical, chemical, and biological processes. These methods facilitate precise manipulation of particle morphology, pore dimensions, and surface characteristics, making them well-suited for various applications. One potential application of these materials is their utilization as antimicrobial agents and photocatalysts.[3] For instance, TiO_2, ZnO, Fe_2O_3, Fe_2TiO_5, and Al_2O_3 NPs have

Received: September 16, 2023
Revised: December 5, 2023
Accepted: December 6, 2023
Published: January 1, 2024

been extensively investigated for their potential photocatalytic potential for the degradation of diverse organic pollutants.[4,5]

Among the various metal oxide NPs, ZnO NP is being widely studied for photocatalytic applications due to its low cost, high chemical stability, nontoxicity, and flexibility in synthesis methods.[6] Additionally, ZnO nanocrystallites possess inherent point defects that enable them to exhibit photocatalytic activity under visible light conditions.[7] When metal oxide semiconductors such as ZnO NPs irradiate with a light energy higher than the band gap, electrons jump from the valence band to the conduction band, which creates electron−hole (e^-/h^+) pairs. However, the photogenerated electron−hole (e^-/h^+) pairs in ZnO quickly recombined, which affected the photocatalytic properties of ZnO NPs.[8] One way of reducing this problem is by doping metals and transition metals into ZnO crystals. Doping has been found to enhance the photocatalytic activities of ZnO NPs via the augmentation of surface defects and modification of optical and electrical transitions.[7,9]

Magnesium is a promising candidate for doping into ZnO due to the close similarity in ionic radius between Mg and Zn. This similarity significantly enhances the likelihood of Mg^{2+} incorporation into the crystal lattice of ZnO. Doping with Mg can also extend the absorption wavelength of ZnO from UV to the visible region, resulting in improved organic dye degradation efficiency in the sunlight.[7−9] Literature reports indicated that biosynthesized Mg-doped NPs exhibited enhanced photocatalytic degradation efficiency toward organic dyes under sunlight irradiation. For instance, *Piper guineense* leaf extract-mediated Mg-doped NPs showed the highest percent degradation of MB at 5% Mg ions concentration.[10] It was also found that up to 7.5% Mg-doped ZnO NPs improved rhodamine B dye degradation when exposed to UV−vis light while increasing the amount of Mg ion lowered its photocatalytic activity.[9]

Nanoparticles can also be vital for treating infectious diseases by replacing the currently available antimicrobial drugs. As various studies show, metal and metal oxide NPs synthesized using plant extracts as reducing agents exhibit promising antimicrobial activity against numerous strains of bacteria.[11] Among them, silver NPs, zinc NPs, and copper NPs have been indicated to have potent antibacterial activity. For example, the CuO NPs synthesized using the *Phyllanthus reticulatus* extract have been reported to show significant antibacterial activity against *E. coli*. In addition, ZnO NPs synthesized using the aqueous extract of *Mentha pulegium* have been reported to show high antibacterial activity against antibiotic-resistant *E. coli* and S. aureus, even though higher activities were observed for CuO NPs than ZnO NPs. In addition, the antibacterial activities of green synthesized TiO_2, Fe_3O_4, ZnO, Cu, and Ag NPs from *Artemisia haussknechtii* against the above bacteria were found significant.[12] The utilization of doping techniques has been found to enhance the antimicrobial activity of metal oxide NPs. For instance, the nanosuspension of ZnO doped with Mg exhibited significant antibacterial efficacy against *Escherichia coli* and *Streptococcus mutans*. However, the antibacterial activity slightly diminished as the concentration of Mg increased.[13] Doping ZnO NPs with Mg ions showed enhanced antibacterial activity against *E. coli*, *S. aureus*, and *Proteus*. The effectiveness of the antibacterial activity increased as the concentration of Mg ions within the ZnO NPs increased.[9] Biosynthesized magnesium-doped zinc oxide nanoparticles (Mg-doped ZnO NPs) were examined for their antimicrobial activity against *Staphylococcus aureus*, *Escherichia coli*, and *Pseudomonas aeruginosa*. The results showed that the Mg-doped ZnO NPs displayed larger inhibition zones than the pristine ZnO NPs.[10]

The synthesis environments, as well as the type and amount of secondary metabolites present in plant extracts, are believed to have an impact on the size, shape, optical properties, and stability of NPs. In the present study, our primary objective was to optimize the synthesis parameters, including precursor metal ions, pH of the solution, volume of plant extract, temperature, and duration of the reaction. The aim was to achieve the most efficient synthesis process. To the best of our knowledge, this study represents the first use of the *Lupinus albus* extract in ZnO and Mg-doped ZnO NPs synthesis. The synthesized NPs were evaluated for their potential utilization as photocatalysts and antibacterial agents.

2. MATERIALS AND METHODS

Zinc nitrate hexahydrate ($(Zn(NO_3)_2{\cdot}6H_2O)$, with a purity of 99.5%, was obtained from LOBA CHEMIE PVT. LTD, India). Distilled water was utilized for the extraction process. Sodium hydroxide (NaOH, 99.0%, Lab Kemical, India) and magnesium nitrate hexahydrate ($(Mg(NO_3)_2{\cdot}6H_2O)$, 98.0%, Avi Chem Industries, Mumbai, India) were utilized as sources of magnesium to dope zinc oxide nanoparticles (ZnO NPs).

2.1. Apparatus and Instruments. The experiment utilized various equipment such as an oven, a digital balance, a centrifuge, a pH meter, UV−vis spectroscopy (SPECORD-200, Analytik Jena), FT-IR spectrometry (Shimadzu IR-470), XRD (D8 ECO XRD, Bruker), and SEM (JCM-6000Plus).

2.2. Collection and Extraction of Plant Materials. The plant leaf sample was collected from the eastern Gojjam Zone, Motta Town, Ethiopia. After collection, the specimen underwent preliminary washing using tap water, followed by air drying and graining. The powdered plant material was extracted using distilled water while being heated and stirred on a hot plate for 1 h. The sample was then filtered via filter paper, and the extract was stored at 4 °C in the refrigerator for further experimentation.

2.3. Preliminary Phytochemical Analysis. Preliminary phytochemical analysis was conducted on the leaf extract of *Lupinus albus* using established testing protocols. The detailed procedures can be found elsewhere in the literature.[14,15]

2.4. Synthesis of ZnO and Mg-Doped ZnO Nanoparticles. The synthesis of ZnO NPs was performed with slight modifications to the method reported in the literature.[16] A known volume of the leaf extract was added to a 0.1 M zinc nitrate solution while being constantly stirred. Subsequently, 2 M sodium hydroxide was incrementally added dropwise to the solution until it achieved a pH of 10. The mixture was subjected to heating for 1 h while being stirred, leading to the formation of a white precipitate. The precipitate was filtered and washed several times with distilled water to remove impurities. The sample was subsequently subjected to drying in an oven set at a temperature of 60 °C. The synthesized ZnO NPs were characterized through visual observation and UV−vis spectroscopy.[3] Finally, the ZnO NPs formed were examined for their photocatalytic and antimicrobial activities. Since the size, shape, optical properties, and stability of NPs depend on synthesis parameters,[15,17−19] in this study, the concentration of the precursor metal ions, pH of the solution, plant extract volume, and reaction time were optimized. The Mg-doped ZnO NPs were synthesized using a slight

https://doi.org/10.1021/acsomega.3c07093
ACS Omega 2024, 9, 2480−2490

modification of the methods described in the literature.[9] The synthesis of Mg-doped ZnO NPs was carried out by mixing 0.1 M $Mg(NO_3)_2{\cdot}6H_2O$ and $Zn(NO_3)_2{\cdot}6H_2O$ solutions under optimum conditions for ZnO NPs synthesis. The impact of the dopant quantity was assessed by altering the concentration of Mg, ranging from 5% to 7.5% to 10% Mg.

2.5. Characterization of ZnO and Mg-Doped ZnO NPs. The characterization of the synthesized nanoparticles was conducted through various techniques such as visual observation, UV−vis spectroscopy, Fourier transform infrared (FT-IR) spectroscopy, X-ray diffraction (XRD), scanning electron microscopy (SEM), and comparison with existing literature data.

2.5.1. UV−Vis Spectrophotometer. The NPs were characterized by utilizing a double-beam UV−vis spectrophotometer (SPECORD 200 PLUS, Analytik Jena, Germany). Samples of the mixture were collected periodically to monitor the completion of the NP formation. The spectra of the samples were recorded within the wavelength range of 250 to 600 nm, with a resolution of 1 nm.

2.5.2. FT-IR Spectroscopy. Fourier transform infrared (FT-IR) analysis was conducted to characterize the adsorbents and identify the functional groups present in the aqueous extract of the plant that could potentially contribute to the formation of NPs. The NPs were characterized by preparing pellets with potassium bromide (KBr) and analyzing them using an FT-IR spectrophotometer (Shimadzu IR-470, Japan) in the wavenumber range of 4000 to 400 cm^{-1}.

2.5.3. X-ray Diffraction (XRD). The crystallographic structure of the NPs was examined by using X-ray diffraction (D8 ECO XRD, Bruker). The XRD patterns were obtained using a diffractometer (Cu K_α radiation, λ = 1.5406 Å) set to 40 kV, 25 mA, and 2θ ranges of 10°−80°. The average crystallite size (D) was calculated using the Debye−Scherrer formula eq 1[4,20]

$$D = \frac{(0.9 \times \lambda)}{(\beta \times \cos\theta)}(\text{Å}) \tag{1}$$

where λ is the wavelength Cu Kα = 1.5406 Å, β is the full width at half-maximum (rad), and θ is the diffraction angle (degrees).

2.5.4. Scanning Electron Microscope (SEM). The scanning electron microscope (SEM) model JCM-6000Plus was utilized to analyze the morphology of ZnO NPs and Mg-doped ZnO NPs. Powdered NPs were subjected to coating with a conducting metal before being scanned by using a precisely focused electron beam. The examination of surface characteristics entailed the application of secondary electrons produced from the sample's surface.

2.6. Photocatalytic Activity Study. The photocatalytic activity of ZnO and Mg-doped ZnO NPs was investigated using established methodologies described in previous studies.[4,21] The degradation of a 10 mg/L solution of MB (methylene blue) by NPs was investigated under direct solar irradiation. The experiment was conducted between 11:00 and 16:00 in February 2023, during which the average daily temperature was 30 ± 2 °C. First, the MB solution and NPs were subjected to magnetic agitation for 30 min in the dark to attain adsorption−desorption equilibrium. The mixture was subsequently subjected to solar irradiation. A 3 mL suspension was periodically collected and subjected to centrifugation to separate and remove the nanoparticles. The residual concentration of MB was analyzed using a UV−vis spectrophotometer within the wavelength range of 400 to 800 nm to investigate the degradation of MB dye by NPs. All of the above steps were repeated for the MB solution without the NPs for comparison purposes. Finally, eq 2 was utilized to determine the percent (%) of dye degradation

$$\%\text{degradation} = \frac{A_0 - A}{A_0} \times 100 \tag{2}$$

where A_0 and A are the initial and final concentrations of MB, respectively.

2.7. Antimicrobial Assay. The as-prepared ZnO and Mg-doped ZnO NPs were tested for in vitro antimicrobial activity against four bacteria strains (*Escherichia coli*, *Bacillus cereus*, *Salmonella typhi*, and *Staphylococcus aureus*) and one fungal strain (*Candida albicans*) using the agar disc diffusion method[22] at Jimma University Microbiology Laboratory. The test solution was prepared by dissolving the NPs in dimethyl sulfoxide (DMSO) to achieve a 200 mg/mL concentration. The inoculums with identical turbidity at 0.5 McFarland were then swabbed uniformly over the Müeller-Hinton Agar medium with a sterile swab. The filter paper discs (6 mm in diameter, made from Whatman No. 1 filter paper and sterilized in an autoclave at 121 °C for 20 min) were then impregnated with the test samples and placed on the medium at an appropriate distance apart to avoid overlap of zones of growth inhibition. The inhibition zone measurement was conducted in millimeters following a 24 h incubation period at 37 °C, and the results were compared to the standard drug, gentamicin (a positive control). As a negative control, DMSO was employed. The antifungal activity of the NPs against *Candida albicans* was tested similarly, except that clotrimazole was used as the reference drug.

3. RESULTS AND DISCUSSION

3.1. Phytochemical Screening of the *Lupinus albus* Extract. The phytochemicals responsible for the reduction and stability of ZnO and Mg-ZnO NPs are determined via qualitative analysis of the aqueous leaf extract of *Lupinus albus*. The results of the phytochemical screening test demonstrated that the aqueous leaf extract of *Lupinus albus* is a valuable reservoir of secondary metabolites (Table 1). These phytochemicals are polar and play a significant role in NPs production.[23] They reduce zinc ions (Zn^{2+}) by losing electrons, acting as a capping agent, and providing stability to ZnO and Mg-ZnO NPs. Flavonoids comprise the principal constituents of *Lupinus albus*, as indicated in Table 1. Flavonoids, due to their high concentration of hydroxyl

Table 1. Phytochemical Screening of *Lupinus albus* Leaf Extract

S. No.	Phytochemicals	Results (Inference)[a]
1	Flavonoids	++
2	Tannins	+
3	Terpenoid	−
4	Alkaloids	+
5	Saponins	−
6	Phenolic compound	+
7	Glycoside	+

[a]Note: (+) sign indicates presence, (++) indicates high intensity, and (−) absence of phytochemical constituents.

https://doi.org/10.1021/acsomega.3c07093
ACS Omega 2024, 9, 2480−2490

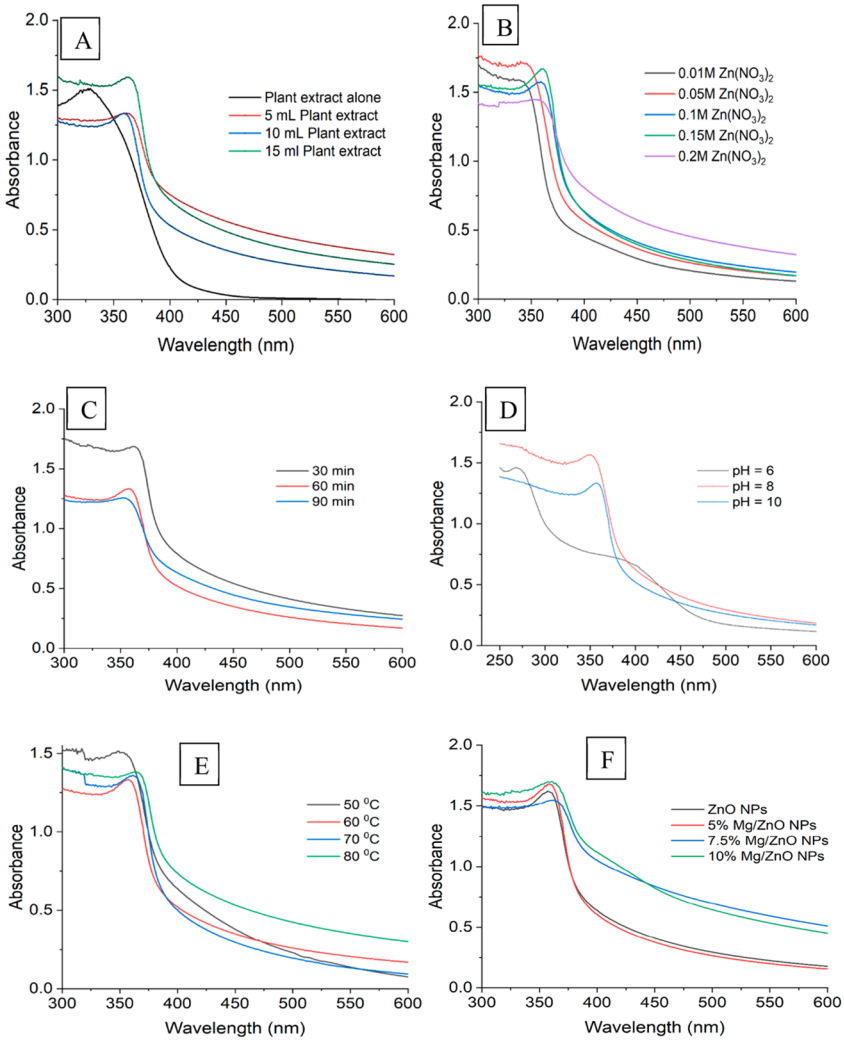

Figure 1. Optimization of the synthesis of ZnO- and Mg-doped ZnO NPs: (A) effect of volume of plant extract, (B) effect of concentration of metal salt precursor, (C) effect of reaction time, (D) effect of pH, (E) effect of temperature, and (F) effect of dopant concentration.

(OH) group, have been found to possess significant effectiveness in reducing and stabilizing zinc ions (Zn^{2+}) at the nanoscale level.[24]

3.2. Optimization of the Synthesis. The morphology of synthesized NPs using plants is significantly influenced by various factors, including the phytochemicals present in the extract, the volume of the extract used, the quantities of precursor metal salt, the pH of the solution, reaction duration, and temperature.[25] Visual inspection and UV−vis spectroscopy were employed to validate the synthesis of the NPs. The UV−vis absorbance of the NPs was measured immediately after preparation and dissolution in water using an ultrasonic bath. The quantity of *Lupinus albus* leaf extract utilized plays a crucial role in zinc ions (Zn^{2+}) reduction in the synthesis of NPs.[26] To ascertain the optimal conditions, various volumes of the extract (5, 10, and 15 mL) were subjected to reaction with a constant quantity of the precursor salt (Figure 1A). The maximum absorption peak of ZnO NPs was observed at approximately 357 nm, which aligns with the findings of a previous study on synthesized ZnO NPs that ranged between 340 and 370 nm.[27] These peaks could be attributed to absorption caused by electrons moving from the lower valence band to the higher conduction band. The absorption spectrum demonstrates a sharp absorbance of around 357 nm, indicating that the NPs were almost uniform in size.[28] However, the observed broadening of the peak suggests that the NPs may have a polydispersed size distribution. The optimal extract volume was determined by selecting the NPs produced using 10 mL of the extract as they exhibited the sharpest peak.

The precursor concentration has been identified as the primary determinant influencing the morphology of ZnO NPs is the precursor concentration.[25,29] Different concentrations of zinc ions were employed in the ZnO NPs synthesis, as depicted in Figure 1B. As the concentration of zinc ions varied from 0.01 to 0.1 M, a noticeable enhancement in the sharpness of the UV−vis absorption peaks was observed. However, further increases in concentration to 0.15 and 0.2 M resulted in peak sharpness reduction. This can be explained by the insufficiency of the phytochemicals in the aqueous leaf extract of *Lupinus albus*, which are responsible for acting as capping agents and stabilizing the nanoparticles. The size of the particles exhibits a positive correlation with the precursor concentration, as supported by previous studies.[30−32]

Reaction time plays a crucial role in the synthesis and stability of NP, as stated by ref 33. The NPs were synthesized at three different reaction times: 30, 60, and 90 min. The formation of ZnO nuclei increases as the reaction time is extended under optimal temperature conditions.[34] As depicted

https://doi.org/10.1021/acsomega.3c07093
ACS Omega 2024, 9, 2480−2490

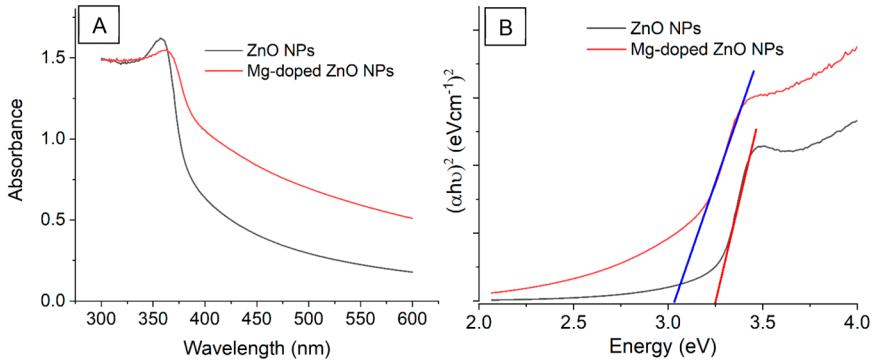

Figure 2. UV−vis spectra (A) and energy band gap (B) of ZnO and Mg-doped ZnO nanoparticles.

in Figure 1C, the graph illustrates that a reaction period of 60 min resulted in a sharp peak, indicating that this is the optimal condition for ZnO NPs synthesis.

The pH level is another influential factor affecting the size, shape, and composition of NPs.[35] The synthesis of ZnO NPs was examined using an aqueous leaf extract of *Lupinus albus* across a pH range of 6 to 10 (Figure 1D). The absence of any color alteration in the solution at pH 6 indicates an insufficient production of ZnO nanoparticles. A redshift and sharp absorption peaks were observed upon increasing the pH from 8 to 10. The rate of ZnO NPs synthesis was higher under alkaline pH conditions than under acidic pH conditions. This difference in the synthesis rate can be attributed to the ionization of the phenolic group present in the extract. The optimal conditions for ZnO NPs synthesis were at pH 10.

Most nanoparticle production processes employ environmentally friendly technologies that demand temperatures below 100 °C or keep them at ambient temperature.[36] The ZnO NPs did not exhibit distinct absorption peaks at 30 and 40 °C (not shown in this paper), suggesting that a negligible quantity of ZnO NPs was produced. The absorption intensities exhibited an upward trend as the temperature was raised from 50 to 60 °C. At 60 °C, a distinct and narrow peak emerged, as depicted in Figure 1E. As the temperature was increased to 70 and 80 °C, the width of the peaks expanded, potentially attributed to the elevated temperature causing accelerated reaction kinetics, unregulated particle size, and rapid aggregation of NPs.[37] Consequently, a temperature of 60 °C was determined to be the optimal condition for ZnO NPs synthesis.

The UV−vis absorption peak of Mg-ZnO NPs was also influenced by the concentration of dopant.[17] ZnO NPs were doped at 5%, 7.5%, and 10% Mg to synthesize Mg-doped ZnO NPs (Figure 1F). The maximum absorbance (λ_{max}) in the UV−vis spectrum broadened and shifted toward longer wavelengths (red-shifted) with an increase in the percentage of dopant up to 7.5% and then decreased when the concentration of Mg increased to 10% while keeping other parameters constant. The UV−vis absorption wavelengths of Mg-doped ZnO NPs with doping concentrations of 5%, 7.5%, and 10% were found to be 358, 363, and 361 nm, respectively. As a result, the optimal value of 7.5% dopant was chosen for the production of Mg-doped ZnO NPs, which aligns with the findings of a previous study.[9]

3.3. Characterization of ZnO and Mg-Doped ZnO NPs. Various characterization techniques, such as visual observation, UV−vis spectroscopy, FT-IR spectroscopy, SEM, and X-ray XRD analysis, were employed to investigate the synthesized nanoparticles. The color change observed in the reaction mixture was utilized as an indicator to track the progress of the synthesis of ZnO and Mg-doped ZnO NPs. The formation of creamy white precipitates during the experimental procedure confirmed the synthesis of ZnO NPs.[30] After the addition of Mg, there was no visible change in the color of the precipitate. The observed red shift in the UV−vis spectrum, specifically from 357 to 363 nm, confirms the doping of ZnO with Mg.

3.3.1. UV−Vis Analysis. The UV−vis absorbance of synthesized ZnO and Mg-doped ZnO NPs was measured within 300−600 nm wavelength. The presence of distinct peaks in the UV−vis spectra at 357 and 363 nm indicates the successful synthesis of ZnO and Mg-doped ZnO NPs, respectively (Figure 2A). When comparing ZnO NPs to Mg-doped ZnO NPs with a doping concentration of 7.5%, it was observed that the absorption edge of the latter was slightly red-shifted toward lower energy. This shift in absorption edge could be attributed to a decrease in the band gap, as suggested by previous report.[38] The Tauc relationship (eq 3)[30] is employed to compute the energy band gap values based on optical absorption spectra.

$$\alpha h_{\nu} = A(h_{\nu} - E_g)^n \quad (3)$$

Where α is the absorption coefficient, h is the plank's constant, ν is the photon frequency, A is a constant, E_g is the band gap, and n is an index that characterizes the optical absorption process (for direct band gap semiconductor material, n = 1/2 and for indirect transition, n = 2). The calculated band gap energies for pristine ZnO NPs and Mg-doped ZnO NPs are 3.25 and 3.02 eV, respectively. These results indicate the successful incorporation of Mg ions into the ZnO lattice. The incorporation of Mg ions into ZnO crystals leads to a reduction in the band gap energy and an expansion of the absorption band, resulting in an enhanced capacity for capturing light. Previous studies have reported conflicting findings regarding the effect of doping ZnO NPs with Mg ions on the band gap. Some studies have found that doping with Mg ions decreases the band gap,[9,39] while others have found that it increases the band gap.[10,13,40,41] The observed discrepancy in the band gap of Mg-doped ZnO NPs can be attributed to several factors, including particle size, oxygen deprivation, surface roughness, and lattice strain.[42]

3.3.2. Fourier Transform Infrared (FT-IR) Analysis. FT-IR analysis was conducted on an aqueous extract of *Lupinus albus*, ZnO, and Mg-doped-ZnO nanoparticles from 400 to 4000

https://doi.org/10.1021/acsomega.3c07093
ACS Omega 2024, 9, 2480−2490

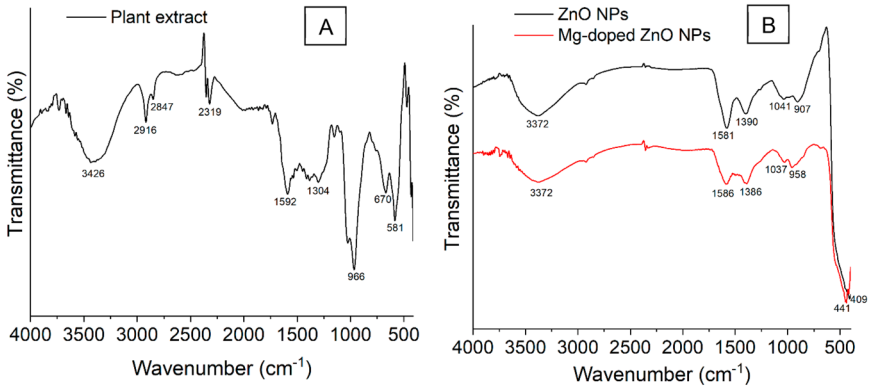

Figure 3. Fourier transform infrared spectroscopy (FT-IR) spectra of (A) *Lupinus albus* extract and (B) ZnO and Mg-doped ZnO NPs.

cm^{-1}. As depicted in Figure 3A, the extract exhibited broad absorption peaks at 3426 cm^{-1}, which can be attributed to the stretching vibration of the −OH group of the phenolic compounds. The peak at 3372 cm^{-1} (Figure 3B) can be attributed to the stretching vibration of the −OH group present on the surface of both ZnO NPs and Mg-doped ZnO NPs. The presence of a weak peak at 2916 cm^{-1} and a slight shoulder peak at 2847 cm^{-1} in the spectrum can be attributed to the stretching vibrations of the asymmetric $-CH_2-$, symmetric $-CH_3$, and $-CH_2-$ groups present in the plant extract. The peak observed at 1592 cm^{-1} can be attributed to the presence of a carbonyl group, while the peak at 1310 cm^{-1} corresponds to C−H bending. The prominent peak observed at 966 cm^{-1} can be attributed to the stretching of the C−O bond. This peak exhibits a decrease in intensity and a shift to 907 and 958 cm^{-1} for ZnO NPs and Mg-doped ZnO NPs, respectively. These observations may suggest that the presence of the carbonyl group plays a role in the reduction and stabilization of the nanoparticles. The absorption peaks at 441 and 409 cm^{-1} (Figure 3B) correspond to the metal−oxygen vibration mode in ZnO NPs and Mg-doped ZnO NPs, respectively.[32]

3.3.3. X-ray Diffraction (XRD) Analysis. The X-ray diffraction pattern was employed to ascertain the crystallinity and distinct phases of the synthesized nanoparticles. The XRD pattern, as shown in Figure 4, exhibits eight well-defined peaks at 2θ values of 31.84°, 34.51°, 36.38°, 47.67°, 56.74°, 63.02°, 68.13°, and 69.22°. These peaks can be attributed to the diffraction planes (100), (002), (101), (102), (110), (103), (112), and (201), respectively. When comparing the data obtained from JCPDS card no. 36-1451 and recently published data,[9,43] it is evident that the intensities and positions of the diffraction peaks indicate the existence of the hexagonal wurtzite crystal structure in the ZnO NPs. The average crystallite size (D) was determined by applying the Debye−Scherrer formula.[4,20] The calculated values for ZnO and Mg-doped ZnO NPs were 28.1 and 34.4 nm, respectively. The diffraction results indicate that there are no significant changes in the XRD patterns of the undoped and Mg-doped ZnO NPs. However, it is observed that the intensity of the peaks decreases after the doping process. These findings indicate a decrease in the crystallinity and the presence of Mg within the ZnO lattice. The findings presented in this study are in line with previous reports.[9,44] The XRD data also indicated that the synthesized NPs exhibit polydispersity as a result of agglomeration or aggregation occurring during the processes of synthesis, storage, or analysis.

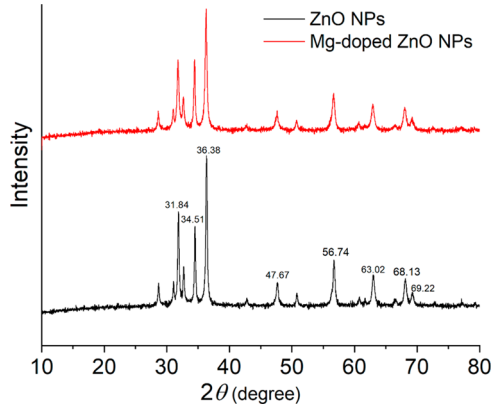

Figure 4. XRD pattern of ZnO and Mg-doped ZnO nanoparticles.

3.3.4. Scanning Electron Microscope (SEM) Analysis. The Scanning electron microscopy (SEM) is a valuable technique for comprehending the morphology of the NPs. Figure 5 gives the surface morphology of the synthesized ZnO NPs and Mg-doped ZnO NPs using *Lupines albus* leaf extract. The surface of undoped ZnO NPs (Figure 5A) is rough compared to that of Mg-doped ZnO NPs (Figure 5B). The particle size of Mg-doped ZnO NPs looks smaller than that of the pristine one, and higher aggregation is observed for Mg-doped ZnO NPs. These differences in surface morphology may be due to the incorporation of Mg ions into the ZnO lattice.

3.4. Antimicrobial Activity Test. The disc diffusion method was used to test the antimicrobial activity of the synthesized NPs against five microorganisms (*S. aureus, B. cereus, S. typhi, E. coli*, and *C. albicans*). The antimicrobial activity of the tested samples was assessed by preparing a 200 mg/mL solution for each sample and measuring the diameter of the zone of inhibition in millimeters. Figure 6 illustrates the inhibition zone of ZnO and Mg-doped ZnO NPs against various Gram-negative and Gram-positive bacteria. As evidenced by the data presented in Table 2, it can be observed that both ZnO NPs and Mg-doped ZnO NPs exhibit antibacterial properties against both Gram-positive and Gram-negative bacteria. However, Mg-doped ZnO NPs induced a higher inhibition zone in comparison to the ZnO NPs. The diameter of the inhibition zone for ZnO NPs ranged from 17 to 21 mm, whereas for Mg-doped ZnO NPs, it ranged from 21 to 24 mm. Particle size has a significant effect on the

https://doi.org/10.1021/acsomega.3c07093
ACS Omega 2024, 9, 2480−2490

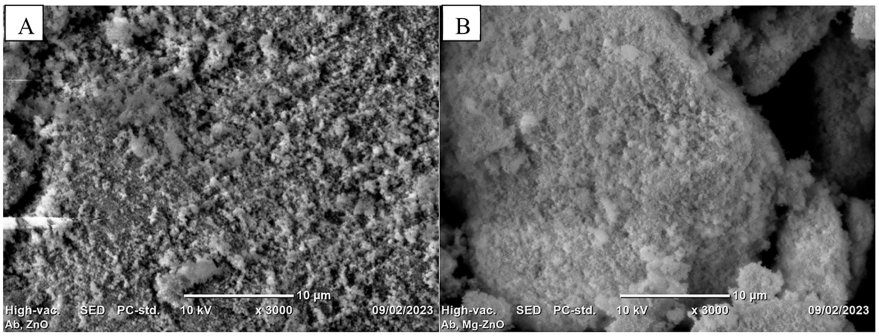

Figure 5. SEM images of (A) ZnO and (B) Mg-doped ZnO nanoparticles.

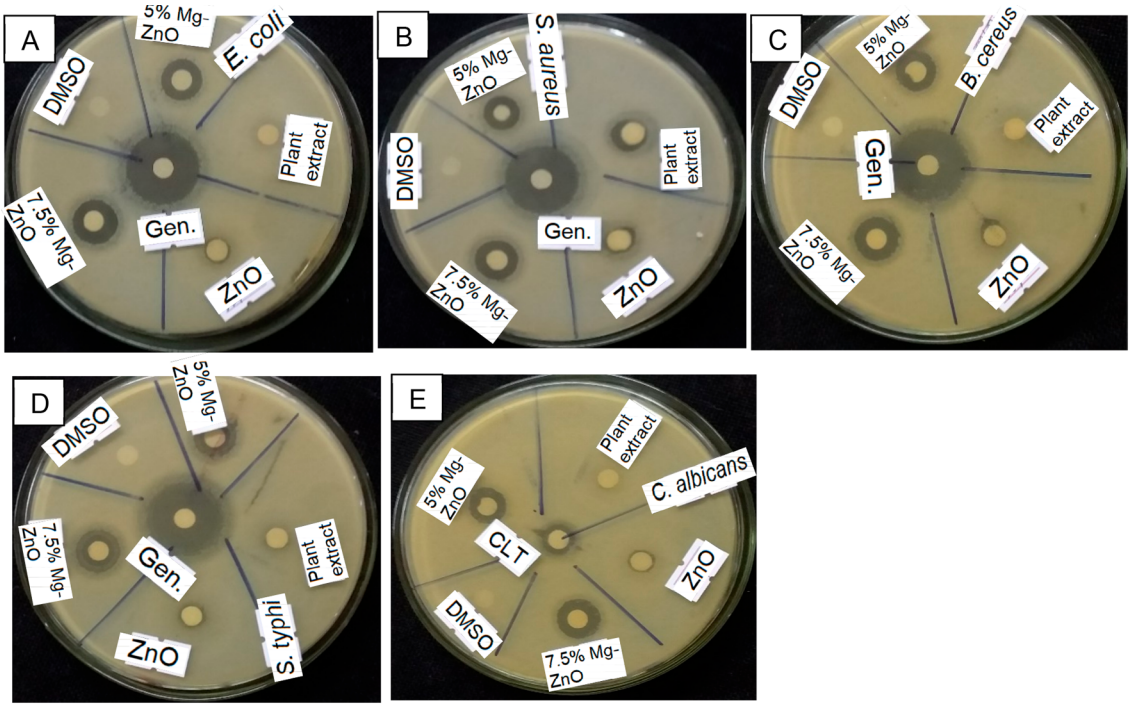

Figure 6. In vitro antimicrobial activities of ZnO NPs, Mg-doped ZnO NPs (5% and 7.5% Mg), plant extract, and negative and positive controls: (A) *E. coli*, (B) *S. aureus*, (C) *B. cereus*, and (D) *S. typhi*, and (E) *C. albicans*.

Table 2. In Vitro Antimicrobial Activities of NPs (Diameter of Zone of Inhibition (mm))

Strains	Leaf Extract	ZnO NPs	Mg-Doped ZnO NPs	Gentamycin	Clotrimazole[a]
E. coli	14	21	24	27	N
S. typhi	13	19	22	28	N
S. aureus	12	17	21	26	N
B. cereus	11	18	21	30	N
C. albicans	10	13	15	N	17

[a]N = Not tested.

antimicrobial activity of NPs. It has been observed that reducing the particle size enhances the antimicrobial activity of ZnO NPs.[45] However, in this study, it was observed that Mg-doped ZnO NPs with a larger particle size of 34.4 nm demonstrated superior antibacterial activity compared to that of ZnO NPs with a smaller particle size of 28.1 nm. The NPs exhibited significant antifungal activity against *Candida albicans*. Specifically, the Mg-doped ZnO NPs demonstrated superior performance compared with the ZnO NPs and were comparable to the standard antifungal drug Clotrimazole.

Even though the synthesized nanoparticles exhibit efficacy against both Gram-negative and Gram-positive bacteria, it was observed that the activity of ZnO and Mg-doped ZnO NPs against Gram-negative bacteria was superior to that against Gram-positive bacteria. This observed difference may be due to variations in the cellular wall composition of the two pathogens.[46] Gram-positive bacteria have a thicker wall as a protective layer, making the interaction between NPs and cell walls less significant.[47] The antibacterial activity of metal oxides is usually determined by their size, specific surface area, and morphology. The electrostatic interaction between negatively charged bacterial cells and positively charged nanoparticles is critical for the NPs functioning as bactericidal agents.[48]

One possible mechanism for the enhanced antibacterial activity of Mg-doped ZnO NPs is that positively charged Mg^{2+} and Zn^{2+} are released and electrostatically interact with the negatively charged bacterial cell membrane. This interaction damages membrane permeability, resulting in the rapid death

https://doi.org/10.1021/acsomega.3c07093
ACS Omega 2024, 9, 2480−2490

of microorganisms.[49] The other suggested mechanism is when the NPs absorb light energy that is greater than the band gap; the electrons jump from the valence band (e^-) of the NPs to the conduction band, which creates a hole (h^+) in the valence band (Scheme 1). The holes split H_2O molecules (from the suspension of ZnO) into OH^- and H^+.[50] The electrons undergo a reaction with the dissolved oxygen molecules, resulting in the formation of superoxide anion ($O^{2\bullet-}$). This anion then combines with H^+ to generate the $HO_2^\bullet$ radical, ultimately leading to the production of hydrogen peroxide (H_2O_2).[50] Hydrogen peroxide exhibits potent oxidizing properties, leading to the disruption of the cell membrane and subsequent bacterial cell death.

Scheme 1. Generation of Reactive Oxygen Species on the Surface of ZnO NPs[50]

$$ZnO + h\nu \rightarrow e^- + h^+$$

$$h^+ + H_2O \rightarrow HO^\bullet + H^+$$

$$e^- + O_2 \rightarrow \bullet O_2^-$$

$$\bullet O_2^- + H^+ \rightarrow HO_2^\bullet$$

$$HO_2^\bullet + H^+ + e^- \rightarrow H_2O_2$$

The increase in antimicrobial activities observed upon doping ZnO NPs can be attributed to the reduction in the energy band gap, which decreases from 3.25 eV for undoped ZnO NPs to 3.02 eV for ZnO NPs doped with Mg. In the case of Mg-doped ZnO NPs, it is observed that the formation of an electron−hole pair can take place at a lower photon energy compared to pristine ZnO NPs. This phenomenon results in an increased production of hydrogen peroxide (H_2O_2) and consequently leads to a higher rate of cell death.[51]

3.5. Photocatalytic Activity. The ability of ZnO and Mg-doped ZnO nanoparticles to degrade the methylene blue (MB) dye was examined under sunlight irradiation. The degradation of MB dye is characterized by a gradual change in the color of the dye solution from blue to colorless along with a continuous decrease in MB absorption as the irradiation time increases (Figure 7). This observation is consistent with previous studies on the photodegradation of MB by ZnO and metal-doped ZnO NPs.[15] The degradation of MB dye was also studied in the presence of sunlight in the absence of catalysts. As seen in Figure 8, the degradation of the MB dye was negligible in the absence of these catalysts. Previous reports also indicated that a minimal amount of MB is degraded through photolysis under sunlight.[52]

Figure 9A depicts the presence of MB (10 mg/L) in the dark with ZnO and Mg-doped ZnO NPs, MB photolysis in sunlight without ZnO and Mg-doped ZnO NPs, and MB photocatalysis in sunlight with ZnO and Mg-doped ZnO NPs. The adsorption−desorption equilibrium was reached within 60 min, with approximately 10% of MB adsorption achieved. Figure 9A also illustrates the minimal degradation of MB in the absence of a photocatalyst compared to adsorption in the dark. The photodegradation of MB under sunlight irradiation with ZnO and Mg-doped ZnO NPs increased with time (Figure

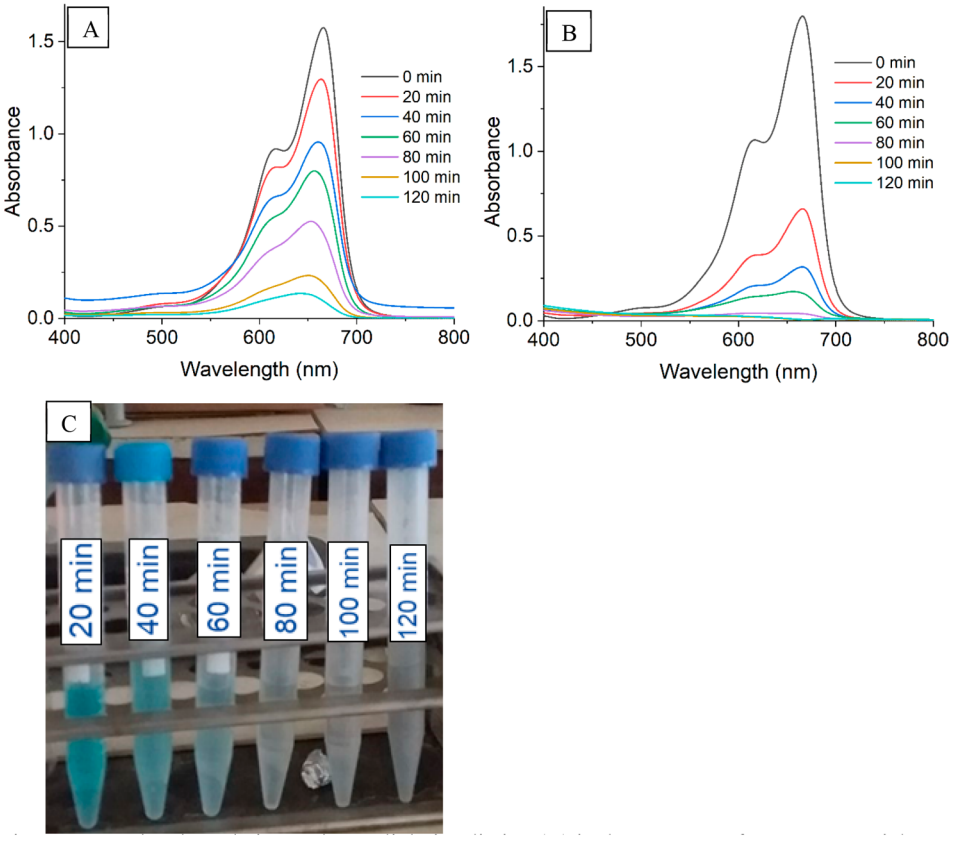

Figure 7. MB dye degradation under sunlight irradiation (A) in the presence of ZnO nanoparticles and (B) in the presence of Mg-doped ZnO nanoparticles; (C) observed color change.

https://doi.org/10.1021/acsomega.3c07093
ACS Omega 2024, 9, 2480−2490

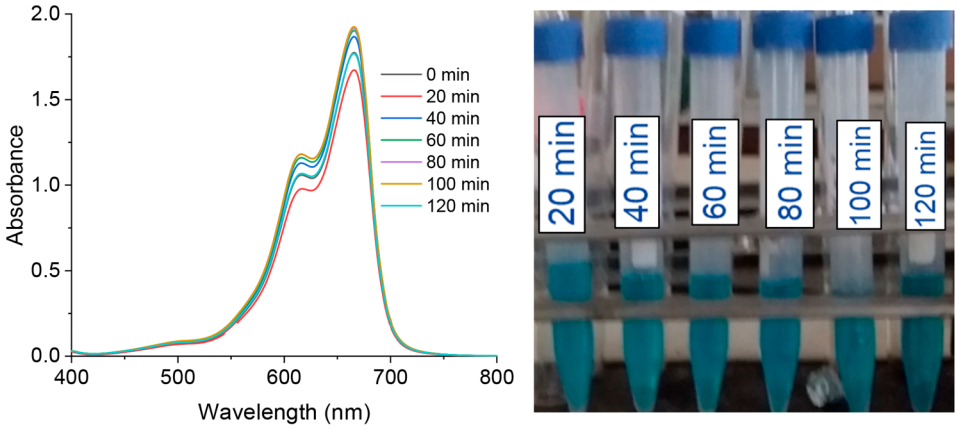

Figure 8. MB dye degradation under sunlight irradiation without using the synthesized NPs.

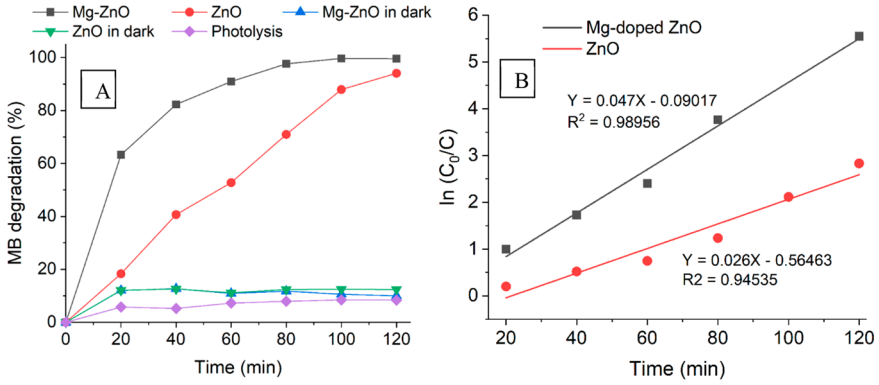

Figure 9. (A) MB dye degradation (10 mg/L) in the presence of ZnO and Mg-doped ZnO NPs in the dark, in sunlight photolysis, photocatalysis in sunlight irradiation, and (B) the reaction kinetics of MB dye degradation for ZnO and Mg-ZnO NPs.

9A). The results showed that Mg-doped ZnO NPs (99.6%) demonstrated better photocatalytic activity than ZnO NPs (94.1%). This enhancement in efficiency was attributed to a decrease in band gap energy or the formation of defects inside the ZnO crystal while doing it with Mg ions.[9]

The methylene blue degradation rate constant (k) for ZnO NPs and Mg-ZnO NPs was calculated from Figure 9B and found to be 2.6×10^{-2} and 4.7×10^{-2}, respectively. The Mg-ZnO NPs have shown a higher degradation rate constant (k) value, which has significantly increased compared with ZnO NPs. Similar results have also been reported previously.[9] The results of this photocatalytic experiment demonstrated that doping Mg ions increased the photocatalytic activity of the ZnO photocatalyst.

3.6. Conclusions. *Lupinus albus* leaf extract was used to synthesize ZnO and Mg-doped ZnO nanoparticles. The NPs were characterized using SEM, XRD, FT-IR, and UV−vis analyses, and the results were compared to existing data. The absorption peaks at 357 and 363 nm in the UV−vis absorption spectra suggest the production of ZnO and Mg-doped ZnO NPs, respectively. The XRD data show that the crystal structure of ZnO NPs is in the hexagonal wurtzite phase. The average crystallite diameters of ZnO and Mg-doped ZnO NPs were 28.1 and 34.4 nm, respectively. Mg-doped ZnO NPs have better antimicrobial activity compared to that of pure ZnO NPs. In addition, Mg-doping increased the photocatalytic activity of ZnO nanoparticles from 94.1% to 99.6%. The observed increase in the photocatalysis may be due to the narrower energy band of Mg-doped ZnO NPs. The study demonstrated that the synthesized NPs are promising alternative candidates for antimicrobial drugs and photocatalysts that can help reduce environmental pollution caused by organic dyes.

AUTHOR INFORMATION

Corresponding Author

Tsegaye Girma Asere − *Department of Chemistry, College of Natural Sciences, Jimma University, Jimma, Ethiopia;* orcid.org/0000-0003-0126-9098; Email: tsegaye96@gmail.com, tsegaye.asere@ju.edu.et

Authors

Abdu Muhammed − *Department of Chemistry, College of Natural Sciences, Jimma University, Jimma, Ethiopia*

Tamiru Fayisa Diriba − *Department of Chemistry, College of Natural Sciences, Jimma University, Jimma, Ethiopia*

Complete contact information is available at: https://pubs.acs.org/10.1021/acsomega.3c07093

Notes

The authors declare no competing financial interest.

ACKNOWLEDGMENTS

We are grateful to Jimma University for supporting this research.

REFERENCES

(1) Krishna, P. G.; Chandra Mishra, P.; Naika, M. M.; Gadewar, M.; Ananthaswamy, P. P.; Rao, S.; Boselin Prabhu, S. R.; Yatish, K. V.; Nagendra, H. G.; Moustafa, M.; Al-Shehri, M.; Jha, S. K.; Lal, B.; Stephen Santhakumari, S. M. Photocatalytic Activity Induced by Metal Nanoparticles Synthesized by Sustainable Approaches: A Comprehensive Review. *Front. Chem.* **2022**, *10*, 1−21.

(2) Mahady, G. Medicinal Plants for the Prevention and Treatment of Bacterial Infections. *Curr. Pharm. Des.* **2005**, *11*, 2405−2427.

(3) Khan, I. I.; Saeed, K.; Khan, I. I. Nanoparticles: Properties, applications and toxicities. *Arab. J. Chem.* **2019**, *12*, 908−931.

(4) Vasiljevic, Z.Z.; Dojcinovic, M.P.; Vujancevic, J.D.; Jankovic-Castvan, I.; Ognjanovic, M.; Tadic, N.B.; Stojadinovic, S.; Brankovic, G.O.; Nikolic, M. V. Photocatalytic degradation of methylene blue under natural sunlight using iron titanate nanoparticles prepared by a modified sol-gel method: Methylene blue degradation with Fe2TiO5. *R. Soc. Open Sci.* **2020**, *7*, 200708.

(5) U, E. A.; C, N. E. N. C.; C, O. C.; Nadia, A.; C, N. E. N. C. Photocatalytic Activity of Aluminium Oxide Nanoparticles on Degradation of Ciprofloxacin. *Saudi J. Eng. Technol.* **2022**, *7*, 132−136.

(6) Adam, R.E.; Alnoor, H.; Pozina, G.; Liu, X.; Willander, M.; Nur, O. Synthesis of Mg-doped ZnO NPs via a chemical low-temperature method and investigation of the efficient photocatalytic activity for the degradation of dyes under solar light. *Solid State Sci.* **2020**, *99*, 106053.

(7) Baruah, S.; Sinha, S.S.; Ghosh, B.; Pal, S.K.; Raychaudhuri, A.K.; Dutta, J. Photoreactivity of ZnO nanoparticles in visible light: Effect of surface states on electron transfer reaction. *J. Appl. Phys.* **2009**, *105*, 074308 DOI: 10.1063/1.3100221.

(8) Sitthichai, S.; Phuruangrat, A.; Thongtem, T.; Thongtem, S. Influence of Mg dopant on photocatalytic properties of Mg-doped ZnO nanoparticles prepared by sol-gel method,. *J. Ceram. Soc. Japan* **2017**, *125*, 122−124.

(9) Pradeev raj, K.; Sadaiyandi, K.; Kennedy, A.; Sagadevan, S.; Chowdhury, Z. Z.; Johan, M. R. B.; Aziz, F. A.; Rafique, R. F.; Thamiz Selvi, R.; Rathina bala, R. Influence of Mg Doping on ZnO Nanoparticles for Enhanced Photocatalytic Evaluation and Antibacterial Analysis. *Nanoscale Res. Lett.* **2018**, *13*, 229.

(10) Okeke, I.S.; Agwu, K.K.; Ubachukwu, A.A.; Madiba, I.G.; Maaza, M.; Whyte, G.M.; Ezema, F.I. Impact of particle size and surface defects on antibacterial and photocatalytic activities of undoped and Mg-doped ZnO nanoparticles, biosynthesized using one-step simple process. *Vacuum.* **2021**, *187*, No. 110110.

(11) Sharmin, S.; Rahaman, M. M.; Sarkar, C.; Atolani, O.; Islam, M. T.; Adeyemi, O. S. Nanoparticles as antimicrobial and antiviral agents: A literature-based perspective study. *Heliyon.* **2021**, *7*, No. e06456.

(12) Anand, U.; Carpena, M.; Kowalska-Góralska, M.; Garcia-Perez, P.; Sunita, K.; Bontempi, E.; Dey, A.; Prieto, M.A.; Proćków, J.; Simal-Gandara, J. Safer plant-based nanoparticles for combating antibiotic resistance in bacteria: A comprehensive review on its potential applications, recent advances, and future perspective. *Sci. Total Environ.* **2022**, *821*, 153472.

(13) Maddahi, P.; Shahtahmasebi, N.; Kompany, A.; Mashreghi, M. Dopant induced changes in physical properties of ZnO:Mg nanosuspensions: Study of antibacterial activity. *Sci. Iran.* **2013**, *20*, 2375−2381.

(14) Pradeep, A.; Dinesh, M.; Govindraj, A.; Vinothkumar, D.; Ramesh Babu, N. Phytochemical analysis of some important medicinal plants. *Int. J. Biol. Pharm. Res.* **2014**, *5*, 48−50.

(15) Firisa, S. G.; Muleta, G. G.; Yimer, A. A. Synthesis of Nickel Oxide Nanoparticles and Copper-Doped Nickel Oxide Nanocomposites Using Phytolacca dodecandra L'Herit Leaf Extract and Evaluation of Its Antioxidant and Photocatalytic Activities. *ACS Omega.* **2022**, *7*, 44720−44732.

(16) Vidya, C.; Hiremath, S.; Chandraprabha, M. N.; Lourdu Antonyraj, M. A.; Venu Gopal, I.; Jain, A.; Bansal, K. Green synthesis of ZnO nanoparticles by Calotropis Gigantea. *Int. J. Curr. Eng. Technol.* **2013**, 2012−2014.

(17) Sa-nguanprang, S.; Phuruangrat, A.; Thongtem, T.; Thongtem, S. Synthesis, Analysis, and Photocatalysis of Mg-Doped ZnO Nanoparticles. *Russ. J. Inorg. Chem.* **2019**, *64*, 1841−1848.

(18) Muthuvel, A.; Jothibas, M.; Manoharan, C. Synthesis of copper oxide nanoparticles by chemical and biogenic methods: photocatalytic degradation and in vitro antioxidant activity, *Nanotechnol. Environ. Eng. 5* (**2020**). DOI: 10.1007/s41204-020-00078-w.

(19) George, A.; Raj, D. M. A.; Raj, A. D.; Irudayaraj, A. A.; Arumugam, J.; Senthil kumar, M.; Prabu, H. J.; Sundaram, S. J.; Al-Dhabi, N. A.; Arasu, M. V.; Maaza, M.; Kaviyarasu, K. Temperature effect on CuO nanoparticles: Antimicrobial activity towards bacterial strains. *Surfaces and Interfaces* **2020**, *21*, No. 100761.

(20) Doan Thi, T. U.; Nguyen, T. T.; Thi, Y. D.; Ta Thi, K. H.; Phan, B. T.; Pham, K. N. Green synthesis of ZnO nanoparticles using orange fruit peel extract for antibacterial activities. *RSC Adv.* **2020**, *10*, 23899−23907.

(21) Rabbani, M.; Shokraiyan, J.; Rahimi, R.; Amrollahi, R. Comparison of photocatalytic activity of ZnO, Ag-ZnO, Cu-ZnO, Ag, Cu-ZnO and TPPS/ZnO for the degradation of methylene blue under UV and visible light irradiation. *Water Sci. Technol.* **2021**, *84*, 1813−1825.

(22) Balouiri, M.; Sadiki, M.; Ibnsouda, S. K. Methods for in vitro evaluating antimicrobial activity: A review. *J. Pharm. Anal.* **2016**, *6*, 71−79.

(23) Hemlata; Meena, P. R.; Singh, A. P.; Tejavath, K. K. Biosynthesis of Silver Nanoparticles Using Cucumis prophetarum Aqueous Leaf Extract and Their Antibacterial and Antiproliferative Activity against Cancer Cell Lines. *ACS Omega.* **2020**, *5*, 5520−5528.

(24) Karam, S.T.; Abdulrahman, A.F. Green Synthesis and Characterization of ZnO Nanoparticles by Using Thyme Plant Leaf Extract. *Photonics* **2022**, *9*, 594.

(25) Xu, J.; Huang, Y.; Zhu, S.; Abbes, N.; Jing, X.; Zhang, L. A review of the green synthesis of ZnO nanoparticles using plant extracts and their prospects for application in antibacterial textiles. *J. Eng. Fiber. Fabr.* **2021**, *16*, 155892502110462.

(26) Bao, Y.; He, J.; Song, K.; Guo, J.; Zhou, X.; Liu, S. Plant-Extract-Mediated Synthesis of Metal Nanoparticles. *J. Chem.* **2021**, *2021*, 1.

(27) Abdol Aziz, R. A.; Abd Karim, S. F.; Rosli, N. A. The effect of ph on zinc oxide nanoparticles characteristics synthesized from banana peel extract. *Key Eng. Mater.* **2019**, *797*, 271−279.

(28) N. Paper, P. Submission, Synthesis of Zinc Oxide Nanoparticles via Sol − Gel Route and Their Characterization. *Nanoscience and Nanotechnology* **2015**, *5*, 1−6.

(29) Benhammada, A.; Trache, D. Green synthesis of CuO nanoparticles using Malva sylvestris leaf extract with different copper precursors and their effect on nitrocellulose thermal behavior. *J. Therm. Anal. Calorim.* **2022**, *147*, 1.

(30) Jobe, M. C.; Mthiyane, D. M. N.; Mwanza, M.; Onwudiwe, D. C. Biosynthesis of zinc oxide and silver/zinc oxide nanoparticles from Urginea epigea for antibacterial and antioxidant applications. *Heliyon* **2022**, *8*, No. e12243.

(31) Javed, A.; Wiener, J.; Saskova, J.; Müllerová, J. Zinc Oxide Nanoparticles (ZnO NPs) and N-Methylol Dimethyl Phosphonopropion Amide (MDPA) System for Flame Retardant Cotton Fabrics. *Polymers (Basel)* **2022**, *14*, 3414.

(32) Kaningini, A. G.; Azizi, S.; Sintwa, N.; Mokalane, K.; Mohale, K. C.; Mudau, F. N.; Maaza, M. Effect of Optimized Precursor Concentration, Temperature, and Doping on Optical Properties of ZnO Nanoparticles Synthesized via a Green Route Using Bush Tea (Athrixia phylicoides DC.) Leaf Extracts. *ACS Omega* **2022**, *7*, 31658−31666.

(33) Darroudi, M.; Bin Ahmad, M.; Zamiri, R.; Zak, A. K.; Abdullah, A. H.; Ibrahim, N. A. Time-dependent effect in green synthesis of silver nanoparticles. *Int. J. Nanomedicine.* **2011**, *6*, 677−681.

(34) Shinde, V. V.; Dalavi, D. S.; Mali, S. S.; Hong, C. K.; Kim, J. H.; Patil, P. S. Surfactant free microwave assisted synthesis of ZnO microspheres: Study of their antibacterial activity. *Appl. Surf. Sci.* **2014**, *307*, 495−502.

https://doi.org/10.1021/acsomega.3c07093
ACS Omega 2024, 9, 2480−2490

(35) Zhang, H.; Chen, B.; Banfield, J. F. Particle size and pH effects on nanoparticle dissolution. *J. Phys. Chem. C* **2010**, *114*, 14876−14884.
(36) Liu, H.; Zhang, H.; Wang, J.; Wei, J. Effect of temperature on the size of biosynthesized silver nanoparticle: Deep insight into microscopic kinetics analysis. *Arab. J. Chem.* **2020**, *13*, 1011−1019.
(37) Mohammadi, F. M.; Ghasemi, N. Influence of temperature and concentration on biosynthesis and characterization of zinc oxide nanoparticles using cherry extract. *J. Nanostructure Chem.* **2018**, *8*, 93−102.
(38) Hafiz, M. M.; Kotb, H. M.; Bakier, Y. M. Determination of Optical Band Gap and Optical Constants of Ge x Sb 40-x Se 60 Thin Films. *Int. J. Thin films Sci. Technol.* **2015**, *185*, 179−185.
(39) Parvizi, E.; Tayebee, R.; Koushki, E. Mg-Doped ZnO and Zn-Doped MgO Semiconductor Nanoparticles; Synthesis and Catalytic, Optical and Electro-Optical Characterization. *Semiconductors* **2019**, *53*, 1769−1783.
(40) Kangathara, N.; Sabari, V.; Saravanan, L.; Elangovan, S. Synthesis, Characterization, and Comparison of Pure Zinc Oxide and Magnesium-Doped Zinc Oxide Nanoparticles and their Application on Ethanol Sensing Activities. *J. Nanomater.* **2022**, *2022*, 1.
(41) Mia, M. N. H.; Pervez, M. F.; Hossain, M. K.; Reefaz Rahman, M.; Uddin, M. J.; Al Mashud, M. A.; Ghosh, H. K.; Hoq, M. Influence of Mg content on tailoring optical bandgap of Mg-doped ZnO thin film prepared by sol-gel method. *Results Phys.* **2017**, *7*, 2683−2691.
(42) Suwanboon, S.; Amornpitoksuk, P. Preparation of Mg-doped ZnO nanoparticles by mechanical milling and their optical properties. *Procedia Eng.* **2012**, *32*, 821−826.
(43) Jayachandran, A.; T. R., A.; Nair, A. S. Green synthesis and characterization of zinc oxide nanoparticles using Cayratia pedata leaf extract. *Biochem. Biophys. Reports.* **2021**, *26*, No. 100995.
(44) R, R.; K, V.; Etacheri, Vinodkumar Mg-Doped ZnO Nanoparticles for Efficient Sunlight-Driven Photocatalysis. *Spectrochim. Acta - Part A Mol. Biomol. Spectrosc* **2014**, *130*, 581−590.
(45) Abebe, B.; Zereffa, E.A.; Tadesse, A.; Murthy, H. C. A. A Review on Enhancing the Antibacterial Activity of ZnO: Mechanisms and Microscopic Investigation. *Nanoscale Res. Lett.* **2020**, *15*, 190 DOI: 10.1186/s11671-020-03418-6.
(46) Shah, A.; Haq, S.; Rehman, W.; Waseem, M.; Shoukat, S.; Rehman, M.U. Photocatalytic and antibacterial activities of paeonia emodi mediated silver oxide nanoparticles. *Mater. Res. Express.* **2019**, *6*, 045045.
(47) Crisan, M.C.; Teodora, M.; Lucian, M.; aCrisan, M. C.; Teodora, M.; Lucian, M. Copper Nanoparticles : Synthesis and Characterization, Physiology, Toxicity and Antimicrobial Applications. *Physiol* **2022**, *12*, 141.
(48) Magdalane, C. M.; Kaviyarasu, K.; Vijaya, J. J.; Siddhardha, B.; Jeyaraj, B. Photocatalytic activity of binary metal oxide nanocomposites of CeO2/CdO nanospheres: Investigation of optical and antimicrobial activity. *J. Photochem. Photobiol. B Biol.* **2016**, *163*, 77−86.
(49) Kasi, G.; Seo, J. Influence of Mg doping on the structural, morphological, optical, thermal, and visible-light responsive antibacterial properties of ZnO nanoparticles synthesized via co-precipitation. *Mater. Sci. Eng. C* **2019**, *98*, 717−725.
(50) Padmavathy, N.; Vijayaraghavan, R. Enhanced bioactivity of ZnO nanoparticles - An antimicrobial study. *Sci. Technol. Adv. Mater.* **2008**, *9*, 035004.
(51) Aga, K. W.; Efa, M. T.; Beyene, T. T. Effects of Sulfur Doping and Temperature on the Energy Bandgap of ZnO Nanoparticles and Their Antibacterial Activities. *ACS Omega.* **2022**, *7*, 10796−10803.
(52) Khare, P.; Singh, A.; Verma, S.; Bhati, A.; Sonker, A. K.; Tripathi, K. M.; Sonkar, S. K. Sunlight-Induced Selective Photocatalytic Degradation of Methylene Blue in Bacterial Culture by Pollutant Soot Derived Nontoxic Graphene Nanosheets. *ACS Sustain. Chem. Eng.* **2018**, *6*, 579−589.

https://doi.org/10.1021/acsomega.3c07093
ACS Omega 2024, 9, 2480−2490